Middle East Journal of Applied Sciences **Volume : 10 | Issue :03 |July-Sept.| 2020**
EISSN: 2706 -7947 ISSN: 2077- 4613 **Pages: 479-489**
DOI: 10.36632/mejas/2020.10.3.42

Enhancing the Electrochemical Performance of Spinel Zinc Stannate by Mixing with Natural Activated Carbon as Energy-Storage Material

M.M. Morad[1], R.M. AbouShahba[1] and M.M. Rashad[2]

[1]Chemistry Department, Faculty of Science (Girls), Al-Azhar University, Cairo, Egypt.
[2]Central Metallurgical Research & Development Institute (CMRDI), Helwan, Cairo, Egypt.

Received: 15 April 2020/ Accepted 22 June 2020 / Publication date: 30 July 2020

ABSTRACT

This paper aims to the evaluation the electrochemical properties of spinel zinc stannate (Zn_2SnO_4) and the enhancement of this performance by mixing it with different ratios of naturally prepared activated carbon from pomegranate peels, Zn_2SnO_4 nano-octahedron-like structure was prepared by facile hydrothermal method using NaOH as a mineralizer. The resulted powder was then mixed with different ratios of naturally prepared activated carbon. The characterization of the as-prepared Zn_2SnO_4 powder revealed a surface area of 49.5 m²/g. Further morphological, optical and electrochemical properties were analyzed by field emission scanning electron microscope, UV–Vis spectroscopy, and the electrochemical techniques. The as-synthesized Zn_2SnO_4 exhibited a specific capacitance of 212 F g^{-1} at 1 A g^{-1} while the optimum ratio is 10%AC+90%Zn_2SnO_4 hybrid composite exhibited 558 F g^{-1} at 1 A g^{-1} which means that capacitance of the Zn_2SnO_4 improved by mixing with 10 % activated carbon, indicating an outstanding improvement of the electrochemical storage capability with capacitance retention of 87% after 2000 cycles at a current density of 10 A g^{-1}. Meanwhile, the practical asymmetrical hybrid-device results show a specific capacitance value of 48.6 F g^{-1} at 1 A g^{-1}, E_d of 19.5 Wh kg^{-1}, and P_d of 1047.7 W kg^{-1} with capacitance retention of 80% of the initial capacitance after 2000 cycles at a current density of 10 A g^{-1}. Overall, these results demonstrate that the enhancement of Zn_2SnO_4 behavior was considered with the addition of the activated carbon on the electrochemical performance of the supercapacitor application.

***Keywords*:** Naturally activated-carbon; Zinc stannate: Asymmetric hybrid supercapacitors; Energy storage.

Introduction

Fuel crisis and ecological deterioration have been considered as an important problem, thus most of researchers and countries tend to have a solution to the energy crisis as an alternative solution such as solar energy, wind energy and also the presence of materials in which the energy is stored for a period of time until it is used (Lewis, 2016; Park *et al.,* 2016 and Zuo *et al.,* 2017.) However, electrical energy storage has become one of the important issues which lead to better utilization of sustainable energies in the future. Therefore, in comparison to batteries, supercapacitors (SCs) are the emerging energy storage technology, because of their ability to store and release energy instantaneously, long life, lower cost, and high-power density with excellent cycle stability. SCs have many applications such as electric vehicles, consumer electronics, portable devices, and wherever a burst of energy supply is required (Shah *et al.,* 2018; Guo *et al.,* 2019 and Wang *et al.,* 2019). SCs are used in applications, where the need to store is or release a huge amount of energy in a very short time. Nowadays, SCs are used primarily in hybrid electric vehicles, electric vehicles, fuel cell vehicles, uninterruptible power supplies, and volatile memory backups in personal computers. The further area of SCs use is energy harvesting systems, solar arrays, or wind turbines, where SCs play a supplementary role next to conventional batteries (Libich *et al.,* 2018*;* Goodenough *et al.*, 2007; Negre *et al.,* 2015; Motlova, 2014; Zhang *et al.,* 2015; Zhang, 2017; Conway and Pell, 2003; Simon and Gogotsi, 2010 ; Naoi and Morita, 2008; Shukla *et al.,* 2012; Zhang *et al.,* 2009; Yu *et al.,* 2013; Lin and Wu, 2011 and Stević, and Rajčić-Vujasinović, 2006). Electrochemical capacitors or ultra-capacitors have many types such as electrochemical double-layer capacitors (EDLCs), Pseudocapacitors, and battery-type SCs. EDLCs store charge either electrostatically or via a non-faradic process, which involves no transfer of charge between the electrode and the electrolyte (Kiamahalleh *et al.,* 2012; Jayalakshmi and Balasubramanian,

Corresponding Author: M.M. Morad, Chemistry Department, Faculty of Science (Girls), Al-Azhar University, Cairo, Egypt. E-mail: monyam19@yahoo.com

2008). In contrary to, pseudocapacitors which store charges via the faradic process, hence, there is charge transfer between electrode and electrolyte (Iro *et al.,*2016). Hybrid capacitor combines both types of EDLs and battery-type SCs, the hybrid SCs can achieve higher energy and power densities with good cycling stability by collecting both Faradaic and non-Faradaic processes to store the charges (Tan and Lee, 2013). Most researches today focus on the production or creation of electrodes from high-energy storage materials such as semiconductor oxides. Zinc stannate (Zn_2SnO_4) is considered an important ternary semiconductor oxide material due to its high electron mobility, high electrical conductivity, low visible light absorption, and attractive optoelectronic properties. Zn_2SnO_4 was reported as a potential material in various applications such as solar cells, gas sensors, Li-ion batteries, and photocatalytic applications (Tan *et al.,* 2007; Oh *et al.,* 2014; Wang *et al.,* 2014; Zhu *et al.,* 2017; Wang *et al.,* 2015 ; Qin *et al.,* 2015; Firooz *et al.,* 2010 and Rasoulifard *et al.,* 2016) . During the last decade, various techniques were developed to synthesize Zn_2SnO_4 nanoparticles such as thermal evaporation (Wang *et al.,* 2005 and Wang *et al.,* 2004). Sol-gel, (Kurz *et al.,* 2006 and Fu *et al.,* 2002. mechanochemical synthesis (Nikolic *et al.,* 2004.). co-precipitation (An *et al.,* 2015 and Wang *et al.,* 2007). and hydrothermal route (Jaculine *et al.,* 2013 and Rong *et al.,* 2006). The hydrothermal technique provides an effective way to fabricate high purity and well crystallized Zn_2SnO_4 phase, also hydrothermal process does not require high reaction temperature which is favorable in the synthesis of Zn_2SnO_4 nanoparticles. It is known that ZnO evaporates easily at high temperature, therefore, techniques work with high temperatures are not valid for Zn_2SnO_4 phase synthesis (Ali *et al.,* 2015; Baruah and Dutta, 2011). In this work, the synthesis of Zn_2SnO_4 and usage as an electrode material for SC applications are reported. The structural, morphological, surface area, optical properties, and electrochemical properties of Zn_2SnO_4 synthesized by the hydrothermal method were studied. The novelty in this work is the preparation of spinel Zn_2SnO_4 without any impurities, testing its electrochemical properties as an SC electrode, and improving the electrochemical behavior by forming composites with different percentage of naturally prepared activated carbon with a high surface area which improved energy life storage. This study aims to investigate and evaluate the low-cost electrode materials for SC application, The addition of naturally activated carbon by ratio 10% to Zn_2SnO_4 improved the capacitance value from 212 F g^{-1} at 1 A g^{-1} for blank Zn_2SnO_4 to 558 F g^{-1} at 1 A g^{-1} for 10%AC+90% Zn_2SnO_4 hybrid composite which exhibited excellent electrochemical performance with a remarkable specific capacitance with good cycling stability of 87% capacitance retention after 2000 cycles at a current density of 10 A g^{-1} which improved the electrode energy-storage life.

Material and Method

1. Experimental procedures

1.2. Preparation of Zn_2SnO_4 nanoparticles.

All the reagents were of analytical grade purchased from Sigma-Aldrich, For the successful synthesis of Zn_2SnO_4 nanoparticles, 2.195g of $Zn(CH_3COO)_2.2H_2O$ and 1.128 g of $SnCl_2.2H_2O$ were dissolved in 100 mL of deionized water separately and then both the solutions were mixed together under constant stirring, followed by dropwise addition of 0.3M NaOH (as a mineralizer) solution into the mixture until a white slurry precipitate was formed at pH 8. Then the mixture was transferred into a 200 mL Teflon coated autoclave and kept at a hydrothermal temperature at 250 ^oC for 48 h. After the hydrothermal reaction, the product was washed with deionized water and ethanol several times and dried. Then the sample was calcined at 400 ^oC for 1h.

1.3. Materials characterization

The as-prepared Zn_2SnO_4 was characterized by powder X-ray diffraction (XRD, Brucker D8 diffractometer) using the Cu-Kα (λ=1.5406 Å) radiation and secondary monochromator in the range 2θ from 10° to 70° and scan rate of 2° min^{-1}. The morphologies were characterized by field emission scanning electron microscope (FE-SEM) using a JEOL instrument (JSM –5410, Japan). The chemical compositions and the valence states of the elements were determined by X-ray photoelectron spectroscopy (XPS, thermos scientific) using Al Kα monochromatized radiation. The specific surface areas were calculated by the Brunauer–Emmett–Teller (BET) method (using Quanta chrome NovaWin - Data Acquisition and Reduction for NOVA instruments ©1994-2013, Quanta chrome Instruments version 11.03).

1.4. Optical properties

The optical properties of the prepared Zn_2SnO_4 nanoparticle were studied using UV–Vis scanning spectrophotometer. The UV–Vis absorption spectrum was recorded by a UV–Vis–NIR scanning spectrophotometer (Jasco-V-570 Spectrophotometer, Japan) using a 1 cm path length quartz cell.

1.5 Electrochemical measurements

The electrochemical performance was studied using a three-electrode system which involves the active material as a working electrode, a platinum wire as a counter electrode, and a saturated calomel electrode (SCE) as a reference electrode. The electrolyte used was 6M KOH. The electrochemical data were collected using (Volta lab 40 PGZ 301, Radiometer Analytical, France) at the room temperature, the working electrode was obtained by mixing the prepared active material with carbon black (conductive additive) and Nafion as a binder in a weight ratio of 80:10:10 respectively, then 0.5 mL of ethanol was added to the mixture to produce a suspended solution. The working electrode was made-up by a drop-casting method in which the suspended solution dropped into nickel foam substrate (NF, Xiamen Tob New Energy Technology Co. LTD, China) with the dimensions of 1 cm (width), 2 cm (length), and 1.6 mm (thickness). For practical simulation, the asymmetric hybrid device was tested in which 90%Zn_2SnO_4 +10%AC electrode was used as a positive electrode and naturally prepared activated carbon as a negative electrode. Activated carbon was prepared from pomegranate peels. Firstly, the peels were carbonized at 850°C for 2h, then crushed with KOH (4-fold weight for the carbonized sample) after that the resulted carbonized powder was heated in a tubular horizontal furnace at different temperatures and times. Initially, it was heated at 200°C for 60 min with nitrogen flow of 150 mL min^{-1}, the temperature was raised to 500°C for 60 min, and then also raised to 850°C with a heating rate of 5°C min^{-1} for 100 min (Dobashi *et al.,* 2015) . Finally, black powder was obtained and used as a negative electrode. The device was denoted as (90% Zn_2SnO_4 +10% AC)//AC). The electrochemical measurements were performed using cyclic voltammetry (CV), galvanostatic charge-discharge (GCD), and electrochemical impedance spectroscopy (EIS) measurements. The CV measurements were carried out within a potential window of -0.1 to 0.6V (vs SCE) at different scan rates from 10 to 200 mV s^{-1}. GCD measurements were tested at different current densities from 1 to 10 A g^{-1} within a potential window of 0 to 0.46 V (vs SCE). The EIS measurements were performed in the frequency range of 100 kHz to 0.01 Hz using Nyquist plots. The stability test was carried at current density 10 A g^{-1}. The specific capacitance (Csp, F g^{-1}) was then calculated from the GCD results according to the following equation (Abdel-Aal *et al.,* 2019 and Mai *et al.,* 2013).

$$Csp = \frac{2I\int V dt}{m V^2} \quad \ldots\ldots (1)$$

Where I is the applied current (A), Δt is the discharging time (s), V is the potential window (V) and m is the mass of active material (g). For the fabrication of the hybrid SC device, the mass ratio of positive and negative electrodes (m+/ m−) can be calculated by the following equation (Chen *et al.,* 2016).

$$\frac{m^+}{m^-} = \frac{C^-_{SP}\Delta V^-}{C^+_{SP}\Delta V^+} \quad \ldots\ldots (2)$$

Where Csp (-) and Csp (+) are the capacitances of the negative and positive electrode, respectively, and ΔV^- and ΔV^+ are the potential windows of the negative and positive electrode, respectively. The CV measurements of the device were carried out within a voltage window of 0 to 1.6 V at different scan rates from 10 to 200 mV s^{-1}. GCD measurements were tested at different current densities from 1 to 10 A g^{-1} between voltage windows of 0 to 1.6 V. The energy density (Ed) and power density (Pd) of the device were calculated according to the equations, respectively (Dai, C.-S., *et al.,* 2013 and Kong, D., *et al.,* 2015).

$$E_d = \frac{I \int V\,dt}{3.6 \times m} \quad \ldots\ldots (3)$$

$$P_d = \frac{3600 \times Ed}{\Delta t} \quad \ldots\ldots (4)$$

Where E_d is the energy density (Wh kg^{-1}), dt is the discharge time (s), P_d is the power density (W kg^{-1}), and (V) is the operating voltage window of the device.

Results and Discussion

1. Crystal Structural and morphological of the synthesized spinel Zn_2SnO_4 nanoparticle.

From the XRD pattern, Fig.1a, the peaks positioned at 2θ of 17.31°, 28.62°, 33.80°, 35.32°, 41.17°, 54.44°, and 59.83° can be indexed to (111), (220), (311), (222), (400), (511) and (440) planes. All the observed diffraction peaks were in good agreement with the standard data of Zn_2SnO_4 with spinel cubic structure (JCPDS #74-2184), which indicates a good crystallization and a single phase of Zn_2SnO_4 obtained hydrothermally at 250° C for 48h at pH 8 followed by calcination at 400 °C for 1h. These conditions are appropriate to remove minor phases of ZnO and SnO_2 (Walsh *et al.,* 2009 and Wei and Zhang, 2001). Fig.1b shows the XPS of O_{1s}, a mean peak with a small shoulder at high binding energy side is observed. The OI deconvoluted-peak is attributed to lattice oxygen while O_2 is ascribed to surface O_2, O, OH groups, and oxygen vacancies. As shown in Fig. 1c, the peaks can be clearly deconvoluted to two peaks at 1021.5 eV and 1044.5eV, which are consistent with the binding energy of Zn $2p_{3/2}$ and Zn $2p_{1/2}$. The splitting energy of 23 eV between Zn $2p_{3/2}$ and Zn $2p_{1/2}$ is a typical value for Zn^{2+} in the Zn_2SnO_4. Meanwhile, the high-resolution XPS spectra of Sn show two deconvoluted-peaks, $3d_{5/2}$ and $Sn3d_{3/2}$ as shown in Fig. 1d, which are obviously observed at 486.9 eV and 495.5eV, respectively, which correspond to the Sn^{4+} (Qin *et al.,* 2015).

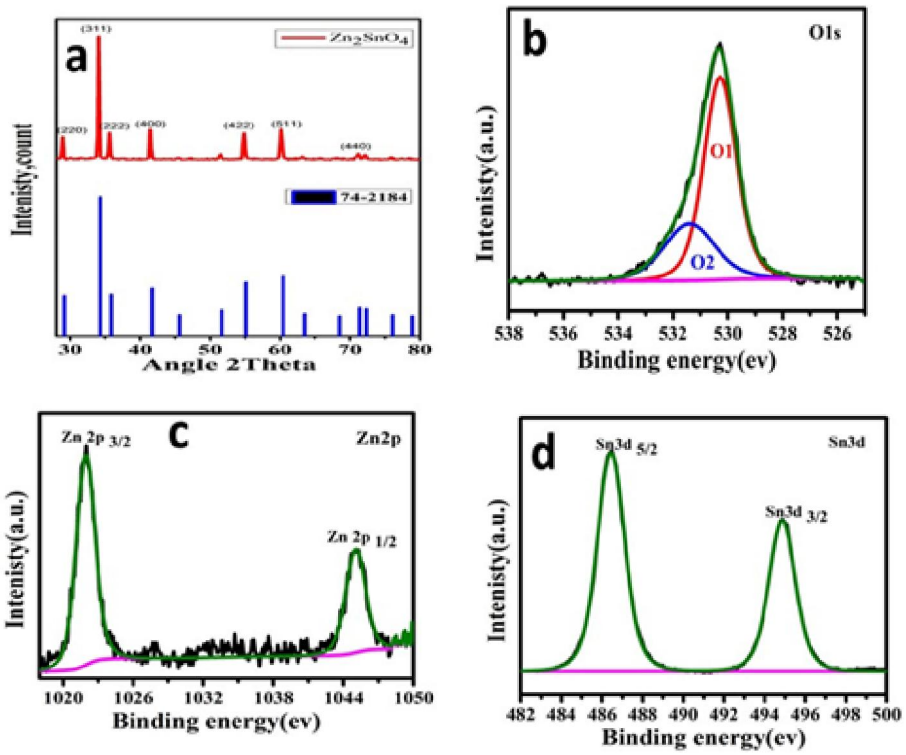

Fig. 1: (a) XRD pattern, and (b, c, d) High-resolution XPS spectra of Zn_2SnO_4.

Fig. 2a and 2b reveal the nitrogen adsorption isotherm of the prepared oxide, The BET surface area was calculated from the nitrogen adsorption isotherm in the P/P_0 range from 0.01 to 0.1 at room temperature, the obtained BET surface area is 49.5 m^2/g. The BET curve exhibits the typical type IV isotherms according to the IUPAC classification (Sing, K.S., 1985). Indicating the mesoporous feature of this sample. The average pore diameter is 8.7nm (Fig. 2b).

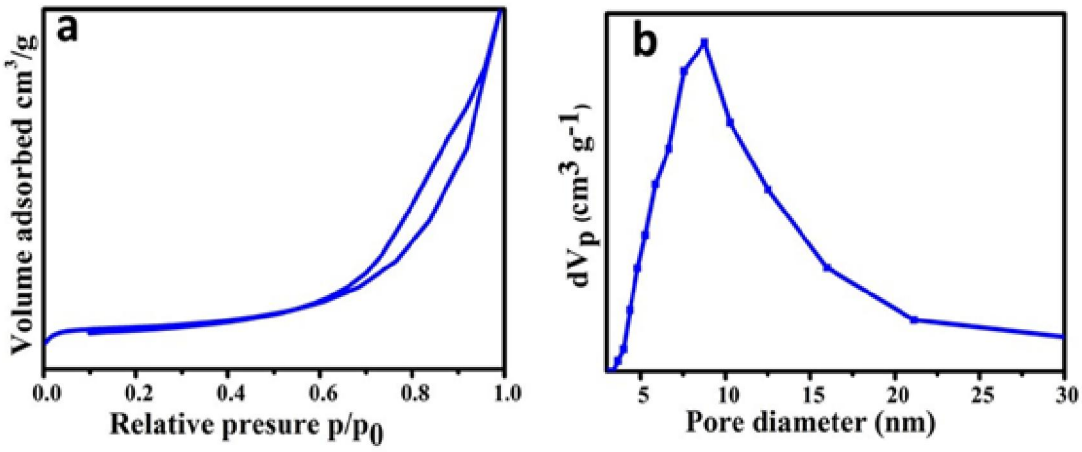

Fig. 2: (a) N_2 adsorption-desorption isotherms and (b) pore size distributions of Zn_2SnO_4.

Fig.3a shows the FESEM image of the as-prepared Zn_2SnO_4, it displays a nano-octahedron-like structure. Fig. 3b, 3c, and 3d show SEM images of different ratios of the composite of natural activated carbon which revealed the formation of octahedron-shaped and some irregular-shaped Zn_2SnO_4–activated carbon nanocomposite.

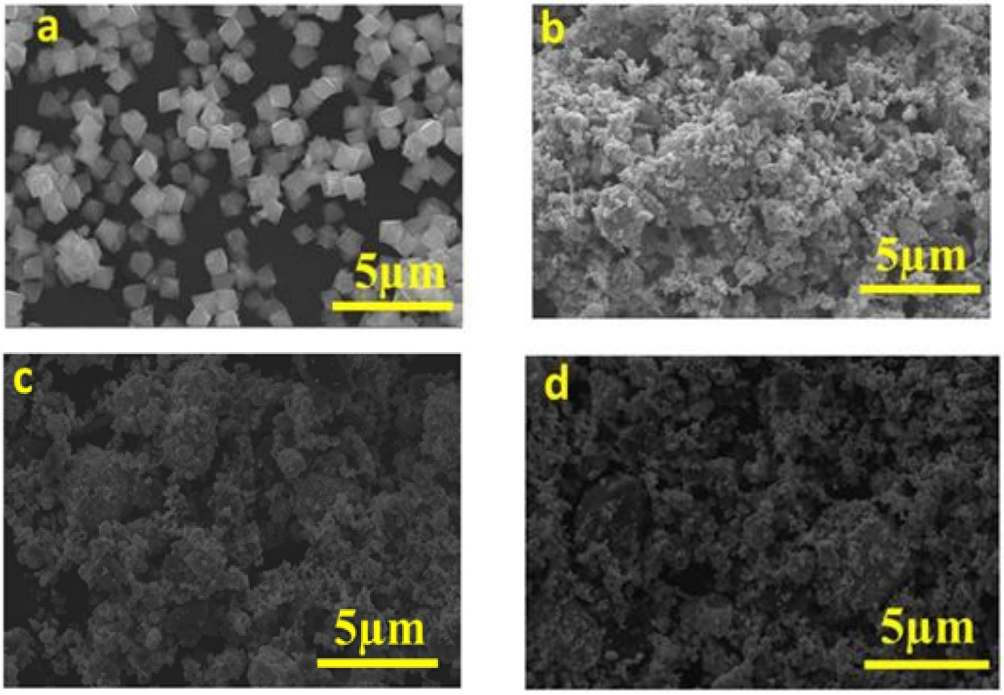

Fig. 3: a) FE-SEM images of the as-prepared Zn_2SnO_4 and, (b), (c), (d) for different ratios of (5,10,15) % Activated carbon mixed with the as-prepared Zn_2SnO_4.

2. Optical properties

Fig.4a shows the absorption spectrum of the prepared Zn_2SnO_4, from the spectrum the maximum absorption was observed at 310 nm, which can be ascribed to Zn_2SnO_4. A similar result was observed by Shi and Dai, 2013). It is clearly observed that the Zn_2SnO_4 has a steep absorption edge, which indicates that the absorption relevant to the bandgap is due to the intrinsic transition of the semiconductors and not because of the transition from impurity levels (Danwittayakul *et al.,* 2013; Tauc

et al., 1966). By using the Tauc formula (Coutts *et al.,* 2000) the optical absorption bandgap can be estimated as

$(\alpha h\upsilon)^{1/n} = K (h\upsilon - Eg)$……. (5)

Where α is the absorption coefficient, hυ is photon energy, K is a constant corresponds to the material, and n depends on the nature of transition in a semiconductor. For allowed direct transition n=1/2 and for indirect transition n=2, it is known that Zn_2SnO_4 is a direct semiconductor and hence, by plotting $(\alpha h\upsilon)^2$ versus hυ the optical band gap, Eg can be determined. Fig.4b shows the Tauc plot for the synthesized Zn_2SnO_4, which gives the bandgap Eg value of 3.16 eV by the intersection of extrapolated linear portion with (hυ) x-axis (Coutts *et al.,* 2000; Fu *et al.,* 2009 and Stoimenov *et al.,* 2002). Zeng *et al.* (2008) have proposed that the fundamental band-gap of Zn_2SnO_4 is 3.6–3.7 eV with a direct-forbidden transition, but a heat treatment on Zn_2SnO_4 narrows the band-gap to 3.25 eV due to the formation and incorporation of excess Zn into the Zn_2SnO_4 crystal (Zeng *et al.,* 2008). In contrast, Young *et al.* (2002) have reported the fundamental band-gap of Zn_2SnO_4 as 3.35 eV, but its bandgap with a high carrier concentration could be widened to 3.89 eV by a Burstein–Moss shift (Young *et al.,* 2002). Previous papers have reported that the band-gap of Zn_2SnO_4 ranges from 3.25 to 3.67 eV (Zeng, *et al.,* 2008 ; Young *et al.,* 2002 ; Zhu *et al.,* 2006 and Cun *et al.,* 2002) . Although the optical absorption property of Zn_2SnO_4 remains controversial, the estimated band-gap value of our single-crystalline Zn_2SnO_4 agrees well with previous reports.

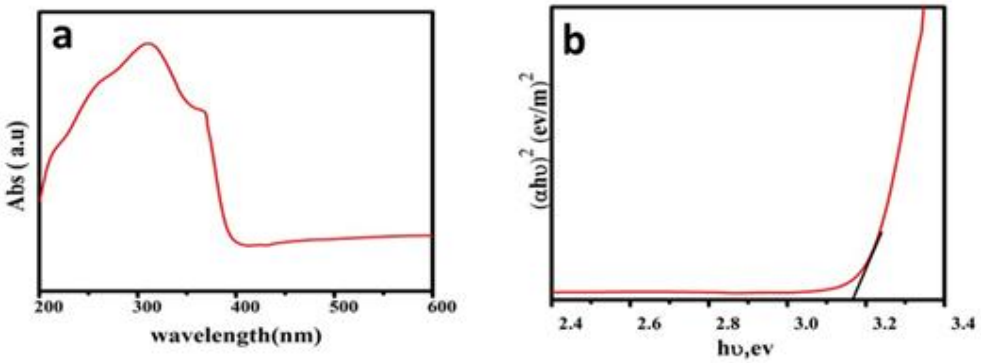

Fig. 4: Please add the figure caption here

3. Electrochemical performance of the supercapacitor electrodes

In order to explain electrochemical behavior of the as-prepared Zn_2SnO_4 and different ratios (5,10,15) % of natural prepared activated carbon mixed with the as-prepared Zn_2SnO_4 to form a composite as an active electrode material for SCs, the CV, GCD, stability, and EIS were measured in 6 M KOH, as shown in Figure 5. It can be seen from Figure 5a that the CV plots of different ratios of Zn_2SnO_4+AC composite and blank Zn_2SnO_4 @50 mV s^{-1} show the presence of well-defined oxidation and reduction peaks suggesting the influence of the faradic reactions in the electrode. For all CV curves, two pairs of redox peaks were noticed within the potential range of -0.1 to 0.6V were matched to each other, these redox peaks are assigned to the reversible redox Faradaic-reaction based on the surface reversible redox-reaction mechanism between Sn(II) and Sn(IV), which is the principle of the typical characteristic of battery-type behavior, this can be based on the following equation (6) (Jin *et al.,* 2018).

$Zn_2SnO_4 + OH^- + H_2O = SnOOH + 2ZnOOH + e^-$…… (6)

From CV plots, it is observed that 10%AC+90%Zn_2SnO_4 composite is considered the best ratio with higher capacitance. In order to quantify the discharge specific capacitance, Fig. 5b shows the charge-discharge profiles of the prepared 10%AC+90%Zn_2SnO_4 hybrid composite and blank Zn_2SnO_4 at current density 1A g^{-1} in the potential range of 0 to 0.46 V. It is clear that the GCD curves exhibit obvious voltage plateaus, indicating that the supercapacitive performance is a Faradic-type.

The presence of plateaus in the curves further confirms the existence of a redox reaction, which is consistent with the results obtained from the CV curves. Csp was calculated from GCD measurements according to equation (1), the calculated capacitance values of 10%AC+90%Zn_2SnO_4 hybrid composite and Zn_2SnO_4 blank electrodes were 558 F g^{-1} and 212 F g^{-1}, respectively, at the current density of 1 A g^{-1}. The capacitance of the 10%AC+90%Zn_2SnO_4 hybrid composite electrode indicates a super improvement of the electrochemical storage capability by mixing with natural prepared activated carbon, these results were better than obtained in the previous works (Jin *et al.,* 2018 and Dinesh *et al.,* 2016). Fig. 5c also illustrates the effect of different current density on the performance of 10%AC+90%Zn_2SnO_4 hybrid composite electrode, it is clear that all GCD curves exhibit obvious voltage plateaus, further demonstrating the Faradic-type supercapacitive performance. The specific capacitances of 10%AC+90%Zn_2SnO_4 hybrid composite can be calculated from each discharging curve, the calculated values of Csp at different current densities of 1,2,3,4,5 and 10 A g^{-1} are 559, 449,398,363,331and 265 F g^{-1}, respectively. It is clearly observed that the specific capacitance decreases gradually with increasing discharge current density because of the charge storage inhibition of some active sites on the surface of the active material at a high current density (Cai *et al.,* 2016). Fig. 5d illustrates the cycling life which was performed based on GCD measurements, which reveals the cycling stability of 10% AC+90% Zn_2SnO_4 hybrid composite electrode at 10 A g^{-1} for 2000 cycles. Remarkable cycling stability of 10% AC+90% Zn_2SnO_4 hybrid composite is attained with 87% capacitance retention being stable even after 2000 cycles. EIS was obtained at the open-circuit voltage and the corresponding Nyquist plots are displayed in Fig. 5f.

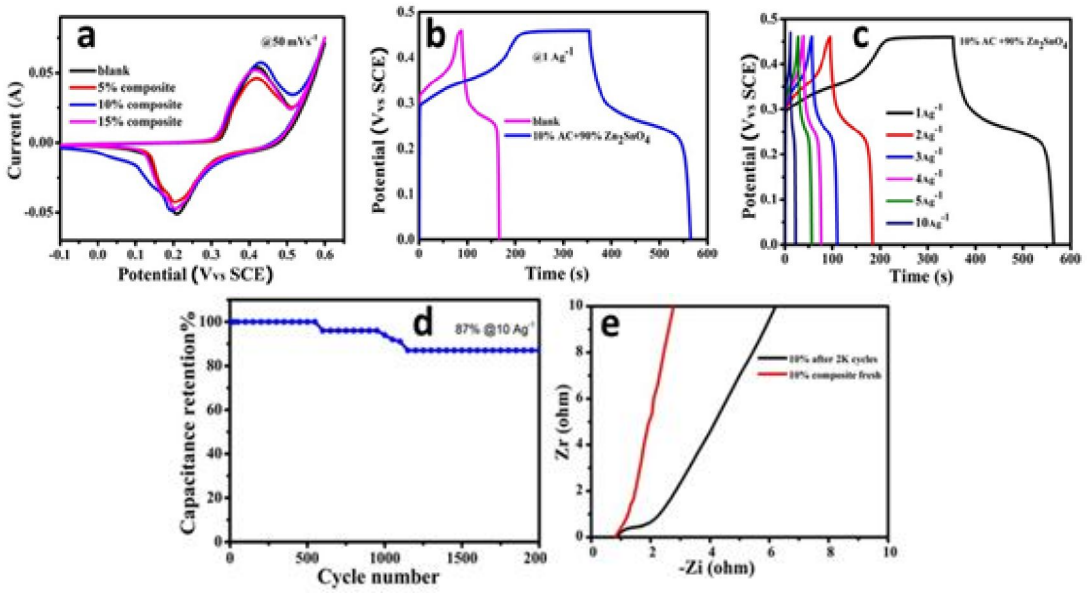

Fig. 5: (a) CV curves at scan rate from 50 mV s^{-1} (b) GCD at current density 1 A g^{-1} for blank Zn_2SnO_4 and 10 % composite (c) Cycling stability of at a current density of 10 A g^{-1}, and (d) EIS profile of 10% composite electrode.

At the high-frequency region, the intersection of the curve at real part (Zr) represents the equivalent series resistance (ESR), which is related to ionic resistance of the electrolyte, internal resistance of the electrode active material, and the contact resistance between the electrode and the current collector (Ito *et al.,* 2015) . From the plots, 10% AC+90% Zn_2SnO_4 hybrid composite as a fresh electrode shows the value of ESR (0.88 ohm) lesser than the one after stability test (0.97 ohm), indicating the absence of the Ohmic loss upon cycling due to high conductivity of AC electrode. The Nyquist plots show a semicircle in the high-frequency region and a near-vertical line at low frequency. The near-vertical line in the low-frequency region indicates the good capacitive-behavior of the 10%AC+90%Zn_2SnO_4 hybrid composite electrode.

4. Asymmetric (hybrid) practical device tested.

Asymmetric-device was tested in a 6M KOH electrolyte using two-electrodes configuration, 10%AC+90%Zn_2SnO_4 hybrid composite as a positive electrode and naturally prepared AC as a negative electrode. To estimate the capacitance of this device, the mass ratio of the positive and negative electrode materials is 3.5 according to the mass balance equation (Eq. 2) (Csp (+) was calculated from the GCD profile (Fig. 5b). The operation potential of the prepared device can be considered as the sum of the potential windows of 10% AC+90% Zn_2SnO_4 (-0.1 to 0.6 V) and AC (-1 to 0 V), therefore, an operation potential window of 0 to 1.7 V was used. The CV curves recorded at different scan rates from 10 mV s^{-1} to 200 mV s^{-1} for asymmetric SC in the potential range of 0 to 1.7 V are shown in Figure 6a. As shown in Fig. 6a in all CV curves of the asymmetrical device presents the redox peaks that were still noticeable in all CV curves, indicating the Faradic-type (battery-like) behavior of the 10%AC+90%Zn_2SnO_4 composite//AC hybrid device. As shown in Fig. 6b, GCD measurements of the device were performed at different current densities of 1, 2, 3, 4, 5, 10 A g^{-1}, The nonlinear charge-discharge profile additionally indicates the battery-type behavior. The device result shows a specific capacitance value of 48.6 F g^{-1}, Ed of 19.5 Wh kg^{-1} and Pd of 1047.7 W kg^{-1} at a current density of 1 A g^{-1}. The cycling stability of the as-fabricated hybrid device was performed by repeating the GCD test within 0 to 1.7 V at a current density of 10 A g^{-1}. As shown in Fig. 6c, the hybrid device of 10%AC+90% Zn_2SnO_4 composite /AC exhibits stability of 80% capacitance retention of the initial capacitance after 2000 cycles, indicating the worthy reversibility and stability of the hybrid device. EIS was also conducted, as shown in Fig. 6d, which showed a lower ESR (1.3 Ohm).

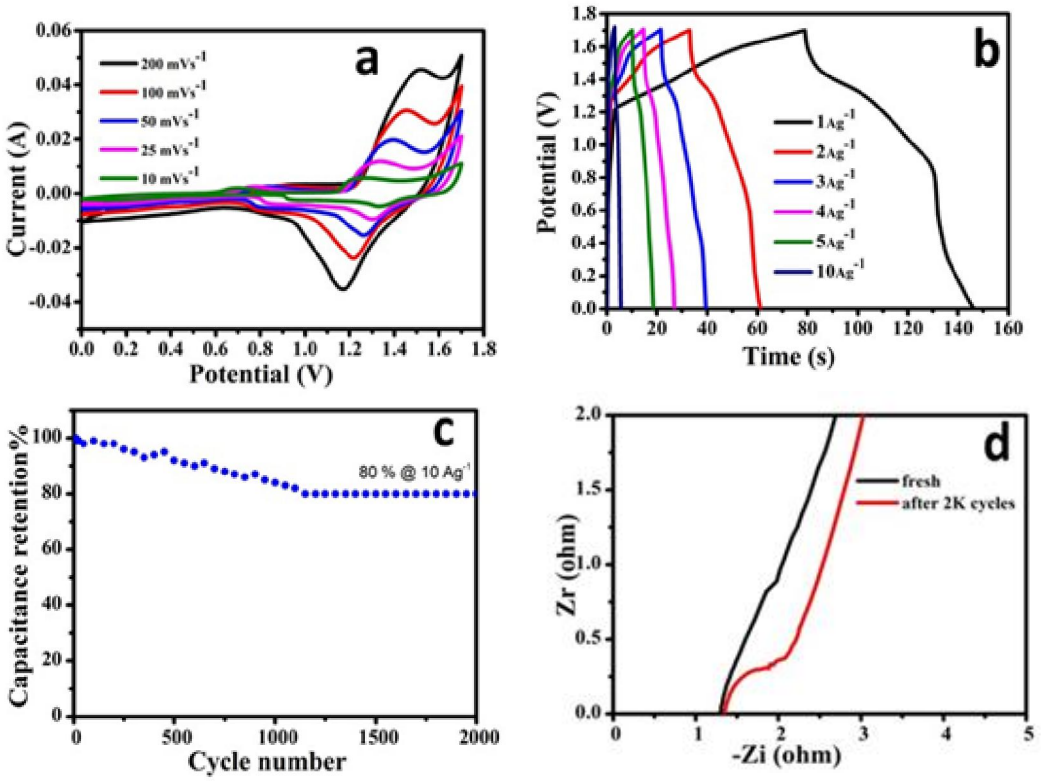

Fig. 6: Electrochemical performance of the 10%AC+90%Zn_2SnO_4 composite //AC hybrid device (a) CV curves at different scan rates, (b) GCD curves at different current densities, (c) cycling performance at a current density of 10 A g^{-1} and (d) EIS for the fresh device and after 2K cycles.

It was observed that ESR slightly changed (1.4 Ohm) after 2000 cycles, indicating a negligible Ohmic loss upon cycling. Finally, Electrochemical results indicate that the 10%AC+90%Zn_2SnO_4 composite //AC hybrid device working as a battery-type SC and has great potential as energy-storage material.

Conclusion

In summary, due to the good conductivity of the naturally prepared AC and high capacitive Zn_2SnO_4, a different ratio of Zn_2SnO_4/AC composites are successfully prepared by well mixing. The prepared Zn_2SnO_4 obtains a specific capacitance value of 212 F g^{-1} at 1 A g^{-1} while the optimum ratio is 10%AC+90% Zn_2SnO_4 hybrid composite exhibits 558 F g^{-1} at 1 A g^{-1} which indicates the capacitance of the Zn_2SnO_4 improved by mixing with 10 % activated carbon, indicating a super improvement of the electrochemical storage capability with capacitance retention of 87% after 2000 cycles at a current density of 10 A g^{-1}. Meanwhile, the practical simulation of asymmetrical hybrid device results shows specific capacitance value of 48.6 F g^{-1}, Ed of 19.5 Wh kg^{-1} and Pd of 1047.7 W kg^{-1} at a current density of 1 A g^{-1}, with capacitance retention of 80% of the initial capacitance after 2000 cycles at a current density of 10 A g^{-1}, from this results Zn_2SnO_4 with a nano-octahedron-like structure loaded with AC could be used for high-performance SCs application.

References

Abdel-Aal, S.K., S.Y. Attia and S.G. Mohamed, 2019. Facile Synthesis of Mn 3 O 4-rGO Nanocomposite as an Efficient Electrode Material for Application in Supercapacitors. Journal of Electronic Materials, 48(8): 4977-4986.

Ali, M.B., *et al.,* 2015. Hydrothermal synthesis, phase structure, optical and photocatalytic properties of Zn2SnO4 nanoparticles. Journal of colloid and interface science, 457: 360-369.

An, D., *et al.,* 2015. Synthesis of Zn2SnO4 via a co-precipitation method and its gas-sensing property toward ethanol. Sensors and Actuators B: Chemical, 213: 155-163.

Baruah, S. and J. Dutta, 2011. Zinc stannate nanostructures: hydrothermal synthesis. Science and technology of advanced materials, 12(1): 013004.

Cai, G., *et al.,* 2016. Ultra-large optical modulation of electrochromic porous WO 3 film and the local monitoring of redox activity. Chemical science, 7(2): 1373-1382.

Chen, T., *et al.,* 2016. All-solid-state high performance asymmetric supercapacitors based on novel MnS nanocrystal and activated carbon materials. Scientific Reports, 6: 23289.

Conway, B. and W. Pell, 2003. Double-layer and pseudocapacitance types of electrochemical capacitors and their applications to the development of hybrid devices. Journal of Solid State Electrochemistry, 7(9): 637-644.

Coutts, T.J., *et al.,* 2000. Search for improved transparent conducting oxides: A fundamental investigation of CdO, Cd 2 SnO_4, and Zn_2SnO_4. Journal of Vacuum Science & Technology A: Vacuum, Surfaces, and Films, 18(6): 2646-2660.

Cun, W., *et al.,* 2002. Synthesis, characterization and photocatalytic property of nano-sized Zn 2 SnO 4. Journal of Materials Science, 37(14): 2989-2996.

Dai, C.-S., *et al.,* 2013. Hierarchically structured Ni3S2/carbon nanotube composites as high performance cathode materials for asymmetric supercapacitors. ACS applied materials & interfaces, 5(22): 12168-12174.

Danwittayakul, S., *et al.,* 2013. Enhancement of photocatalytic degradation of methyl orange by supported zinc oxide nanorods/zinc stannate (ZnO/ZTO) on porous substrates. Industrial & Engineering Chemistry Research, 52(38): 13629-13636.

Dinesh, S., *et al.,* 2016. Effect of activated carbon on electrochemical and photocatalytic performance of hydrothermally synthesized zinc stannate nanoparticles. Journal of Materials Science: Materials in Electronics, 27(12): 12786-12795.

Dobashi, A., *et al.,* 2015. Preparation of activated carbon by KOH activation from amygdalus pedunculata shell and its application for electric double-layer capacitor. Electrochemistry, 83(5): 351-353.

Firooz, A.A., *et al.,* 2010. High photocatalytic activity of Zn_2SnO_4 among various nanostructures of $Zn_2xSn1{-}xO_2$ prepared by a hydrothermal method. Chemical engineering journal, 165(2):735-739.

Fu, G., *et al.,* 2002. Humidity sensitive characteristics of Zn2SnO4–LiZnVO4 thick films prepared by the sol–gel method. Sensors and Actuators B: Chemical, 81(2-3): 308-312.

Fu, X., *et al.,* 2009. Hydrothermal synthesis, characterization, and photocatalytic properties of Zn_2SnO_4. Journal of Solid State Chemistry, 182(3): 517-524.

Goodenough, J.B., H. Abruna, and M. Buchanan, 2007.Basic research needs for electrical energy storage. in Report of the basic energy sciences workshop for electrical energy storage.

Guo, Y., *et al.,* 2019. Functional Hydrogels for Next-Generation Batteries and Supercapacitors. Trends in Chemistry ,

Iro, Z.S., C. Subramani, and S. Dash, 2016. A brief review on electrode materials for supercapacitor. Int. J. Electrochem. Sci., 11(12): 10628-10643.

Ito, Y., *et al.,* 2015. High catalytic activity of nitrogen and sulfur co-doped nanoporous graphene in the hydrogen evolution reaction. Angewandte Chemie International Edition, 54(7): 2131-2136.

Jaculine, M.M., C.J. Raj and S.J. Das, 2013. Hydrothermal synthesis of highly crystalline Zn2SnO4 nanoflowers and their optical properties. Journal of Alloys and Compounds, 577: 131-137.

Jayalakshmi, M. and K. Balasubramanian, 2008. Simple capacitors to supercapacitors-an overview. Int. J. Electrochem. Sci, 3(11): 1196-1217.

Jin, K., *et al.,* 2018. Zn_2SnO_4/activated carbon composites for high cycle performance supercapacitor electrode. Journal of Alloys and Compounds, 767: 419-423.

Kiamahalleh, M.V., *et al.,* 2012. Multiwalled carbon nanotubes based nanocomposites for supercapacitors: a review of electrode materials. Nano, 7(02): 1230002.

Kong, D., *et al.,* 2015. Three-dimensional Co3O4@C@Ni3S2 sandwich-structured nanoneedle arrays: towards high-performance flexible all-solid-state asymmetric supercapacitors. Journal of Materials Chemistry A., 3(31): 16150-16161.

Kurz, A., *et al.,* 2006. Strategies for novel transparent conducting sol–gel oxide coatings. Thin Solid Films, 502(1-2): 212-218.

Lewis, N.S., 2016. Research opportunities to advance solar energy utilization. Science, 351(6271): aad1920.

Libich, J., *et al.,* 2018. Supercapacitors: Properties and applications. Journal of Energy Storage, 2018. 17: 224-227.

Lin, Y.P. and N.L. Wu, 2011. Characterization of $MnFe_2O_4$/$LiMn_2O_4$ aqueous asymmetric supercapacitor. Journal of Power Sources, 196(2): 851-854.

Mai, L.Q., *et al.,* 2013. Synergistic interaction between redox-active electrolyte and binder-free functionalized carbon for ultrahigh supercapacitor performance. Nature communications, 4(1): 1-7.

Motlova, D., 2014. Aplikace elektroanalytickych metod ve studiu purinovych derivatu. Masarykova univerzita, Prirodovedecka fakulta.

Naoi, K. and M. Morita, 2008. Advanced polymers as active materials and electrolytes for electrochemical capacitors and hybrid capacitor systems. The Electrochemical Society Interface, 17(1): 44-48.

Negre, L., *et al.,* 2015. Solvent-free electrolytes for electrical double layer capacitors. Journal of the Electrochemical Society, 162(5): A5037-A5040.

Nikolic, N., Z. Marinkovic, and T. Sreckovic, 2004. The influence of grinding conditions on the mechanochemical synthesis of zinc stannate. Journal of materials science, 39(16-17): 5239-5242.

Oh, L.S., *et al.,* 2014. Zn2SnO4-based photoelectrodes for organolead halide perovskite solar cells. The Journal of Physical Chemistry C, 118(40): 22991-22994.

Park, M., *et al.,* 2016. Material design and engineering of next-generation flow-battery technologies. Nature Reviews Materials, 2(1): 1-18.

Qin, L., *et al.,* 2015. Facile solvothermal synthesis of Zn_2SnO_4 nanoparticles as anode materials for lithium-ion batteries. Materials Letters, 141: 255-258.

Qin, Y.L., *et al.,* 2015. Controllable synthesis of cube-like ZnSnO3@ TiO 2 nanostructures as lithium ion battery anodes. Journal of Materials Chemistry A, 3(6): 2985-2990.

Rasoulifard, M., M.S. Dorraji, and S. Taherkhani, 2016. Photocatalytic activity of zinc stannate: preparation and modeling. Journal of the Taiwan Institute of Chemical Engineers, 58: 324-332.

Rong, A., *et al.,* 2006. Hydrothermal synthesis of Zn2SnO4 as anode materials for Li-ion battery. The Journal of Physical Chemistry B, 110(30): 14754-14760.

Shah, H.U., *et al.,* 2018. Synthesis, Characterization and Electrochemical Properties of α-MnO2 Nanowires as Electrode Material for Supercapacitors. Int. J. Electrochem. Sci, 13: 6426-6435.

Shi, L. and Y. Dai, 2013. Synthesis and photocatalytic activity of Zn 2 SnO 4 nanotube arrays. Journal of Materials Chemistry A, 1(41): 12981-12986.

Shukla, A., *et al.,* 2012. Electrochemical capacitors: Technical challenges and prognosis for future markets. Electrochimica Acta, 84: 165-173.

Simon, and Y. Gogotsi, 2010, Materials for electrochemical capacitors, in Nanoscience and Technology: A Collection of Reviews from Nature Journals. World Scientific. 320-329.

Sing, K.S., 1985. Reporting physisorption data for gas/solid systems with special reference to the determination of surface area and porosity (Recommendations 1984). Pure and applied chemistry, 57(4): 603-619.

Stević, Z. and M. Rajčić-Vujasinović, 2006. Chalcocite as a potential material for supercapacitors. Journal of Power Sources, 160(2): 1511-1517.

Stoimenov, P.K., *et al.,* 2002.Metal oxide nanoparticles as bactericidal agents. Langmuir, 18(17): 6679-6686.

Tan, B., *et al.,* 2007. Zinc stannate (Zn_2SnO_4) dye-sensitized solar cells. Journal of the American Chemical Society, 129(14): 4162-4163.

Tan, Y.B. and J.M. Lee, 2013. Graphene for supercapacitor applications. Journal of Materials Chemistry A, 1(47): 14814-14843.

Tauc, J., R. Grigorovici, and A. Vancu, 1966. Optical properties and electronic structure of amorphous germanium. physica status solidi (b), 15(2): 627-637.

Walsh, A., J.L. Da Silva, and S.-H. Wei, 2009. Interplay between order and disorder in the high performance of amorphous transparent conducting oxides. Chemistry of Materials, 21(21): 5119-5124.

Wang, B.-Y., *et al.,* 2015. Facile synthesis of fine Zn2SnO4 nanoparticles/graphene composites with superior lithium storage performance. Journal of Power Sources, 281: 341-349.

Wang, J., *et al.,* 2004. Synthesis, structure, and photoluminescence of Zn2SnO4 single-crystal nanobelts and nanorings. Solid state communications, 131(7): 435-440.

Wang, L., *et al.,* 2005. A simple method to synthesize single-crystalline Zn2SnO4 (ZTO) nanowires and their photoluminescence properties. Nanotechnology, 16(12): 2928.

Wang, S., *et al.,* 2007. Coprecipitation synthesis of hollow Zn2SnO4 spheres. Materials Letters, 61(14-15): 3005-3008.

Wang, T., *et al.,* 2019. Boosting the cycling stability of transition metal compounds-based supercapacitors. Energy Storage Materials, 16: 545-573.

Wang, Y., *et al.,* 2014. Synthesis of 3D-nanonet hollow structured Co3O4 for high capacity supercapacitor. ACS applied materials & interfaces, 6(9): 6739-6747.

Wei, S.H. and S. Zhang, 2001. First-principles study of cation distribution in eighteen closed-shell A II B 2 III O 4 and A IV B 2 II O 4 spinel oxides. Physical Review B, 63(4): 045112.

Young, D.L., *et al.,* 2002. Growth and characterization of radio frequency magnetron sputter-deposited zinc stannate, Zn2SnO4, thin films. Journal of applied physics, 92(1): 310-319.

Yu, G., *et al.,* 2013. Hybrid nanostructured materials for high-performance electrochemical capacitors. Nano Energy, 2(2): 213-234.

Zeng, J., *et al.,* 2008. Transformation process and photocatalytic activities of hydrothermally synthesized Zn2SnO4 nanocrystals. The Journal of Physical Chemistry C, 112(11): 4159-4167.

Zhang, J., *et al.,* 2015. Pre-lithiation design and lithium ion intercalation plateaus utilization of mesocarbon microbeads anode for lithium-ion capacitors. Electrochimica Acta, 182: 156-164.

Zhang, S.S., 2017. Eliminating pre-lithiation step for making high energy density hybrid Li-ion capacitor. Journal of Power Sources, 343: 322-328.

Zhang, Y., *et al.,* 2009. Progress of electrochemical capacitor electrode materials: A review. International journal of hydrogen energy, 34(11): 4889-4899.

Zhu, B., *et al.,* 2017. Fabrication and photocatalytic activity enhanced mechanism of direct Z-scheme g-C3N4/Ag2WO4 photocatalyst. Applied Surface Science, 391: 175-183.

Zhu, H., *et al.,* 2006. Hydrothermal synthesis of Zn2SnO4 nanorods in the diameter regime of sub-5 nm and their properties. The Journal of Physical Chemistry B, 110(15): 7631-7634.

Zuo, W., *et al.,* 2017. Battery-supercapacitor hybrid devices: recent progress and future prospects. Advanced Science, 4(7): 1600539.